Convective invigoration traced to warm-rain microphysics

Xin Rong Chua^{1,1} and Yi $Ming^{2,2}$

¹Centre for Climate Research Singapore ²Geophysical Fluid Dynamics Laboratory

November 30, 2022

Abstract

Aerosols are postulated to alter moist convection by increasing cloud droplet number concentration. Cloud-resolving model simulations of radiative-convective equilibrium show that increased cloud droplet number concentration leads to higher convective mass flux, seemingly in line with a popular hypothesis which links the convective invigoration to delayed rain formation allowing more cloud liquid water to be frozen. Yet, the same phenomenon is also present in an alternative model configuration with only warm-rain microphysics, suggesting that one does not have to invoke ice microphysics. The key mechanism lies in the different vertical distributions of the increases in cloud liquid re-evaporation and in water vapor condensation, causing a dipole pattern that favors convection. This is further supported by a mechanism-denial experiment in which weakened cloud re-evaporation tends to mute invigoration. This work represents a major advancement of the process-level understanding of aerosol effects on convection.

Convective invigoration traced to warm-rain microphysics

Xin Rong Chua^{1*}, Yi Ming^{1,2}

4	¹ Program in Atmospheric and Oceanic Sciences, Princeton University, Princeton, New Jersey, USA
5	² Geophysical Fluid Dynamics Laboratory/NOAA, Princeton, New Jersey, USA

6 Key Points:

1

2

3

7	• Higher cloud droplet number concentration increases convective mass flux, even
8	in the absence of ice microphysics.
9	• The convective invigoration coincides with higher tropospheric relative humidity
10	and re-evaporation efficiency.
11	• The dynamical mechanism involves a vertical dipole (cooling-above-warming) pat-
12	tern.

 $^{^{*}\}mathrm{Current}$ affiliation: Centre for Climate Research Singapore, Singapore

Corresponding author: Yi Ming, Yi.Ming@noaa.gov

13 Abstract

Aerosols are postulated to alter moist convection by increasing cloud droplet num-14 ber concentration (N_d) . Cloud-resolving model simulations of radiative-convective equi-15 librium show that higher N_d leads to stronger convective mass flux, seemingly in line with 16 a hypothesis that links the convective invigoration to delayed rain formation allowing 17 more cloud liquid condensate to be frozen. Yet, the invigoration is also present in an al-18 ternative model configuration with warm-rain microphysics only, suggesting that ice mi-19 crophysics is not central to the phenomenon. The key dynamical mechanism lies in the 20 different vertical distributions of the increases in water vapor condensation and in cloud 21 liquid re-evaporation, causing a dipole pattern favoring convection. This is further sup-22 ported by a pair of mechanism-denial experiments in which an imposed weakening of cloud 23 liquid re-evaporation tends to mute invigoration. 24

²⁵ Plain Language Summary

Aerosols are thought to affect moist convection by increasing cloud droplet num-26 ber concentration. According to a popular hypothesis, higher droplet number concen-27 tration would delay rain formation, allowing more cloud water to reach the freezing level. 28 The additional latent heating from freezing is presumed to cause stronger convection. 29 We test this hypothesis with a numerical model capable of simulating moist convection, 30 and find that convective invigoration occurs even in the absence of ice processes. A de-31 tailed analysis suggests that the slowdown of rain formation increases cloud liquid re-32 evaporation. The resulting cooling is balanced primarily by stronger water vapor con-33 densation. This creates a vertical cooling-above-warming dipole pattern favorable to con-34 vection. 35

36 1 Introduction

Aerosols, natural and anthropogenic alike, alter Earth's radiative budget by scattering and/or absorbing shortwave radiation, as well as by altering cloud albedo (Twomey, 1974) and lifetime (Albrecht, 1989). Both effects have important implications for moist convection and precipitation. This work focuses on the purely microphysical pathway through which aerosols affect deep convective clouds by increasing cloud droplet number concentration (N_d). A commonly referenced mechanism (Rosenfeld et al., 2008; Williams

-2-

et al., 2002; Andreae et al., 2004) posits that higher N_d leads to smaller droplets, thus delaying rain formation. This effect tends to bring more cloud liquid water above the freezing level, and the additional latent heat release would invigorate convection.

Stevens and Feingold (2009) hypothesized that delayed precipitation formation would 46 allow more liquid to reach the cloud-top region of a cumulus. The resulting re-evaporative 47 cooling has an effect of destabilizing the atmospheric column, and thus promoting con-48 vection. It was also acknowledged that this cloud-dynamical effect might be mitigated 49 by more efficient precipitation production in deep clouds. More broadly, the re-evaporation 50 of cloud condensate, by influencing cold pool strength, can exert a strong control on sub-51 sequent convection (e.g. Tao et al., 2007; Morrison, 2012; Tao et al., 2012). A recent study 52 by Fan et al. (2018) suggested that ultrafine aerosol particles (smaller than 50 nm) can 53 be activated into cloud droplets in a clean environment owing to higher in-cloud super-54 saturation; the additional droplets in return facilitate condensation. It was argued that 55 the resulting convective invigoration occurs via a warm-phase (liquid) microphysical path-56 way based on the relatively small increase in upper-level latent heating. In other words, 57 one does not have to rely on ice microphysics to explain the convective adjustment to 58 aerosols. 59

To further complicate the matter, there is no consensus among the existing case 60 studies on how aerosols would strengthen or weaken convection (see Morrison (2012) for 61 a case of weakening). It is not straightforward to make comparison across different case 62 studies given that environmental factors such as wind shear (e.g. Fan et al., 2009) and 63 cloud-radiative effects (e.g. Fan et al., 2015) can potentially alter the eventual convec-64 tive response. In contrast, the setting of radiative-convective equilibrium (RCE) makes 65 it possible to diagnose which processes are of leading-order importance to the simulated 66 quasi-steady state in a simple framework. For example, van den Heever et al. (2011) found 67 an increase in the frequency of updrafts in response to increased N_d . In a follow-up study 68 focusing on deep convective clouds, Storer and van den Heever (2013) showed that the 69 freezing of cloud liquid is not among the largest contributors to the overall latent heat 70 budget, suggesting that at least in RCE, freezing might not be as important for under-71 standing convective invigoration as initially thought. This study is conceived as a tar-72 geted mechanistic study of the role of liquid microphysics in determining aerosol effects 73 on convection. 74

-3-

75 **2** Methodology

The RCE simulations are performed with the Weather Research and Forecasting 76 (WRF) model (Wang & Sobel, 2011), a widely used cloud-resolving model (CRM). The 77 configuration is identical to that used in Chua et al. (2019) except for the treatment of 78 cloud microphysics (as detailed later). The model domain is doubly periodic and con-79 tains 96×96 gridpoints at a horizontal resolution of 2 km with fifty vertical levels. At-80 mospheric radiative cooling is prescribed at -1.5 K day^{-1} in the troposphere (defined as 81 temperature warmer than 207.5 K). Elsewhere temperature is relaxed to 200 K over 5 82 days following a Newtonian relaxation scheme. Prescribing radiative cooling eliminates 83 a major confounding factor common to this type of studies. Surface sensible and latent 84 heat fluxes are computed with an aerodynamic formulation at a constant near-surface 85 wind speed of 5 m s⁻¹. The surface temperature is set at 301 K. Subgrid diffusion is cal-86 culated with the Smagorinsky and YSU schemes (Hong et al., 2006). Domain-average 87 winds are nudged to zero on a time scale of two hours. 88

The model uses the the double-moment Morrison cloud microphysics scheme (Morrison 89 et al., 2009). By tracking both mass mixing ratios and numbers of hydrometeors, a double-90 moment scheme is deemed to be more suitable for simulating the microphysical effects 91 of aerosols on moist convection than a single-moment scheme of mixing ratios. The warm-92 rain or liquid part of the scheme is described briefly here as it is important for under-93 standing the results. Water vapor (q_v) condenses into cloud liquid (q_l) through satura-94 tion adjustment. Note that q denotes mass mixing ratio. Re-evaporation of cloud liq-95 uid occurs only under subsaturated conditions. Cloud liquid converts into rain (q_r) through 96 either autoconversion or accretion; the rates are parameterized as $1350q_l^{2.47}N_d^{-1.79}$ and 97 $67(q_lq_r)^{1.15}$, respectively (Khairoutdinov & Kogan, 2000). Note that q_l and q_r are in kg 98 kg^{-1} , N_d in cm⁻³ and the rates in kg kg⁻¹ s⁻¹. Autoconversion is the only microphys-99 ical process that is controlled directly by N_d . Rain can re-evaporate back into water va-100 por. 101

Three alternative configurations are created from simplifying the full model (referred to as FU). One can turn off the ice part of the Morrison scheme. In the resulting configuration (referred to as LI), the liquid microphysics operates at all temperatures. The formulae used for computing the cloud liquid and rain re-evaporation rates are scaled

-4-

by a factor of 0.1 in the CE and RE configurations, respectively. This does not mean that
the actual rates would decrease by 10 times as other factors may also vary.

For each of the four model configurations (i.e. FU, LI, CE and RE), a pair of simulations are performed. N_d is set to 100 cm⁻³ in the control experiment, and 1000 cm⁻³ in the perturbation experiment. The former is denoted by the name of a configuration, and the latter by adding an asterisk. For example, the control and perturbation experiments performed with the full model are referred to as FU and FU*, respectively.

A control experiment is initialized from a warm bubble, and is integrated for 240 model days. The output at Day 180 is used to initialize a corresponding 60-day perturbation experiment. We analyze the last 20 days of hourly-mean outputs from each simulation. The noise level of a given variable is quantified using five consecutive, non-overlapping 20-day periods from an extended full model control simulation (namely FU).

118 **3 Results**

Some key characteristics of the control simulations and their changes in response 119 to higher N_d are depicted in Figure 1. The distributions of cloud liquid (q_l) in the lower 120 and mid-troposphere are similar among all four configurations, with a distinct peak at 121 around 900 hPa (Figure 1a). As designed, high clouds are comprised of ice (q_i) in FU, 122 and liquid in the other cases. Interestingly, the upper-tropospheric q_l in LI and CE is 123 comparable to q_i in FU, but much higher than q_l in RE. Higher N_d gives rise to an in-124 crease in cloud condensate below 500 hPa in all cases (Figure 1b). CE is opposite to the 125 other three cases in showing a substantial increase in high cloud condensate. 126

In FU, rain (q_r) is concentrated mostly below 500 hPa, while snow and graupel (col-127 lectively referred to as snow, q_s) dominates above. The three liquid microphysics con-128 trol simulations exhibit almost identical vertical distributions of rain throughout the col-129 umn, which are bottom-heavy with maxima at around 700 hPa (Figure 1c). Elevated 130 N_d causes q_r to decrease in all cases below 600 hPa, and to increase in the three liquid 131 microphysics cases above, albeit to varying degrees (Figure 1d). q_s in FU increases as 132 well. Taken together, the increase in cloud liquid and the concurrent decrease in rain in 133 the lower troposphere are consistent with the microphysical nature of the perturbation, 134 i.e. higher N_d tending to suppress the conversion of cloud liquid to rain, while convec-135 tive adjustment seems to play a prominent role in shaping the upper-tropospheric changes. 136

-5-

Convective mass flux (M_c) is computed by summing the mass flux at gridpoints 137 where the total cloud condensate $(q_c, \text{ or } q_l + q_i)$ is greater than 0.005 g kg⁻¹ and ver-138 tical velocity exceeds 1 m ${\rm s}^{-1}$ (Wang & Sobel, 2011). In much of the troposphere, M_c 139 in FU is substantially (about 40%) stronger than in the liquid microphysics cases (Fig-140 ure 1e). They also differ in vertical structures; FU has only one in the lower troposphere, 141 while the latter have two peaks, one in the lower troposphere and the other in the up-142 per troposphere. M_c shows a substantial increase below 500 hPa due to higher N_d , which 143 amounts to ${\sim}30\%$ at 600 hPa (Figure 1f). The convective invigoration is accompanied 144 by a relatively small decrease in M_c in the upper troposphere in FU^{*} and LI^{*}. The mag-145 nitude of the enhancement of M_c is fully captured in LI, suggesting that ice microphysics 146 is not essential for explaining the convective invigoration, contrary to Rosenfeld et al. 147 (2008). Furthermore, the invigoration is muted in the configuration of CE, indicating 148 that cloud liquid re-evaporation may be a key process involved in the convective response. 149 In contrast, RE does not show any appreciable difference from LI, which hints at a sec-150 ondary role played by rain re-evaporation. Note that none of the simulations examined 151 here shows any sign of self-aggregation. 152

Figure 1g shows the relative humidity (RH) in the control cases. The vertical pro-153 files take a C-shape, with minima at around 500 hPa. FU, however, has notably higher 154 mid-tropospheric RH (\sim 70%) than the liquid microphysics cases (\sim 40%), suggesting that 155 ice microphysics is crucial for moistening the mid-troposphere. A comparison of RE and 156 LI indicates that rain re-evaporation is also an important source of mid-tropospheric mois-157 ture, while cloud liquid re-evaporation is not (CE versus LI). Across all cases, RH shows 158 a pronounced increase below 500 hPa owing to higher N_d (Figure 1h). With the excep-159 tion of CE, they all experience lower RH in the upper troposphere. 160

The impression from Figures 1(f) and (h) that convective invigoration coincides 161 with mid-tropospheric moistening is formalized in Figure 2. The vertically averaged con-162 vective mass flux $([M_c])$ in the various control and perturbation experiments is gener-163 ally positively correlated with the column-average relative humidity (CRH). The cor-164 relation with the mid-tropospheric (400 to 600 hPa) relative humidity (MRH) is even 165 stronger. This relationship holds not only for every pair of control and perturbation ex-166 periments but also for all the control experiments. Although it is well established that 167 a moist mid-troposphere is conducive to convective development (e.g. in the context of 168 tropical cyclones), convective detrainment of cloud condensate is an important supplier 169

of mid-tropospheric moisture. These two mechanisms are not mutually exclusive, and
 work in the same direction. This work does not attempt to address the relative roles of
 these mechanisms, which would be difficult to separate in a clean way.

The need to better understand the controlling factors of RH prompts us to exam-173 ine the moisture budget. The column-integrated source and sink terms, along with the 174 changes caused by increased N_d , are given in Table 1. To facilitate the discussion, they 175 are also illustrated in Figure 3 for the LI configuration. For water vapor, condensation 176 (C) is balanced by surface evaporation (ES), and re-evaporation of cloud condensate and 177 rain (EC and ER, respectively). The conversion from cloud liquid to rain is realized through 178 autoconversion (CR) and accretion (AR). Although autoconversion is almost negligi-179 ble in terms of domain average (consistent with other cloud-resolving simulations (e.g. 180 Heikenfeld et al., 2019)), it is the only process through which rain formation can occur 181 spontaneously – a necessary condition for accretion that involves both cloud liquid and 182 rain simultaneously. In this sense, it is conceivable that a perturbation to the former, 183 however small in magnitude, may still affect the latter. Rain is partitioned between re-184 evaporation (ER) and surface precipitation (P). 185

The re-evaporation efficiency (α) is defined as the ratio of the total re-evaporation 186 (E, or the sum of EC and ER) to C (Romps, 2014). Note that one definition of the widely 187 used quantity called precipitation efficiency is the ratio of surface precipitation (P) to 188 C (e.g. Langhans et al., 2015; Lutsko & Cronin, 2018). Thus, α is one minus the pre-189 cipitation efficiency. Dictated, to the zeroth order, by the free-tropospheric radiative cool-190 ing rate, the domain-average ES or P is little changed regardless of the configurations 191 or perturbations. Both C and E are substantially lower in LI than in FU, but the frac-192 tional decrease in E is greater than that in C. This results in a net decrease in α . As 193 expected, weakening the re-evaporation processes tends to lower α , albeit to different ex-194 tents. α is more sensitive to the perturbation to rain re-evaporation than that to cloud 195 liquid re-evaporation, implying that EC is limited more strongly by the availability of 196 cloud liquid as opposed to the prescribed rate constant. 197

Higher N_d leads to a slowdown in accretion by modulating autoconversion. This is consistent with higher q_l and lower q_r (Figures 1b and d). As explained before, since P is somewhat fixed, and δCR is small, δAR must be approximately equal to δER (with δ denoting changes). This explains why rain re-evaporation decreases. Higher q_l is consistent with stronger EC as they are directly linked. Since P is approximately unchanged, it follows that $\delta C \simeq \delta ER + \delta EC$. This relation, however, does not help constrain the sign of δC as δER and δEC are of opposite signs. It seems plausible to assume that Cand EC would vary in the same direction as they are the dominant sink and source terms in the cloud liquid budget, an issue to which we will return later.

Invoking $\delta C \simeq \delta E$, one can write $\delta \alpha$ approximately as $(1-\alpha)\delta C/(C+\delta C)$. If it is assumed that $\delta C \ll C$, the expression can be further simplified to $\delta \alpha \simeq (1-\alpha)\delta C/C$. This simple theory is found to be in good agreement with the simulated $\delta \alpha$ (Table 1). Thus, the increase in α can be thought of as a manifestation of stronger condensation.

Across all the cases, α is strongly correlated with column relative humidity (CRH) 211 (Figure 2c), and to a lesser extent, with mid-tropospheric relative humidity (MRH) (Fig-212 ure 2d). This result is qualitatively consistent with an analytical model of tropospheric 213 relative humidity in RCE (Romps, 2014), in which cloud condensate re-evaporation is 214 treated as an important mechanism for moistening the environment. In particular, α is 215 smaller than CRH, conforming to the constraint inferred from the analytical model. This 216 line of reasoning appears to suggest that the microphysical perturbation caused by higher 217 N_d tends to increase the re-evaporation efficiency. The resulting tropospheric moisten-218 ing creates a favorable environment for convection. 219

As appealing as the above explanation is, it does not yield insights into the dynam-220 ics underlying the convective invigoration. The microphysical processes discussed above 221 can be divided into two categories depending on whether phase change is involved. The 222 latent heating from condensation (C) and the latent cooling from rain and cloud con-223 densation re-evaporation (ER and EC, respectively) play crucial roles in the energy bal-224 ance, and have to be in equilibrium with other diabatic (e.g. radiative) and dynamical 225 terms (resolved and implicit). In contrast, accretion is not part of the energy balance. 226 Furthermore, the latent heating and cooling have distinct vertical structures as illustrated 227 in Figure 4. In all the control experiments, the condensational heating peaks much lower 228 $(\sim 900 \text{ hPa})$ than the re-evaporative cooling (600 to 700 hPa). Conceptually, the former 229 generates positive buoyancy for lifting an air parcel. As the parcel rises, it entrains drier/colder 230 environmental air and detrains cloud condensate, which then re-evaporates into the en-231 vironment. Similar to condensation, the total heating is bottom-heavy, but with a dis-232 tinct local minimum owing to re-evaporation. 233

Both condensation and cloud liquid re-evaporation are stronger in the perturbed 234 energy balance, with a secondary weakening of rain re-evaporation. Although the com-235 bined effect is integrated vertically to near zero, it is characteristic of a dipole (cooling 236 above warming) structure as δC is more bottom-heavy than δEC . The positive buoy-237 ancy resulting from this pattern is consistent with the enhancement of M_c (Figure 1f). 238 Given that the initial perturbation is applied through modifying cloud liquid, one may 239 speculate that it is the stronger re-evaporative cooling that destabilizes the lower tro-240 posphere and promotes stronger convection (condensation). This explains why conden-241 sation and cloud liquid re-evaporation vary in the same direction, and constitutes a dy-242 namical mechanism of the microphysically induced convective adjustment. 243

244

4 Discussion and Conclusions

As an anchor point of this work, the re-evaporation efficiency (α) is an emergent 245 property of the RCE simulations, and is closely associated with tropospheric relative hu-246 midity and convective mass fluxes across a wide range of model configurations and per-247 turbations. It has been shown that the increase in α due to higher N_d can be linked to 248 stronger condensation by invoking the simple theory $(\delta \alpha \simeq (1 - \alpha) \delta C/C)$, which can 249 also be used to explain, at least qualitatively, the large difference in α among the four 250 control experiments (from 0.368 in RE to 0.664 in FU). Although it is clear from our re-251 sults that the treatment of cloud microphysics has a direct bearing on α , convective dy-252 namics also plays an essential role, as evidenced by the destabilizing effect of cloud liq-253 uid re-evaporation. In light of its importance for understanding tropospheric relative hu-254 midity (Romps, 2014), convectively coupled tropical variations and general circulation 255 (Emanuel, 2019) and climate sensitivity (Zhao et al., 2016), the potential use of α for 256 comparing a variety of model simulations (limited-domain and global CRMs, and coarse-257 resolution global climate models or GCMs) and observations (Noone, 2012) should be 258 explored. 259

A contemporaneous study by Abbott and Cronin (2020) offers a way to examine the robustness of our results to the choice of model configurations and experimental designs. Both studies find that an increase in N_d gives rise to higher mid-tropospheric relative humidity and convective invigoration in RCE simulations, even in the absence of ice microphysics. While this work centers over convective invigoration (manifested as stronger

-9-

convective mass flux) in RCE, Abbott and Cronin (2020) focuses on changes in high-percentile
 vertical velocities under the assumption of weak temperature gradient balance.

Ice microphysical processes are often thought to play a key role in enhancing con-267 vection under polluted conditions. In the setting of RCE with prescribed radiative cool-268 ing, we demonstrate that an increase in cloud droplet number concentration can cause 269 stronger convective mass flux even in the absence of ice microphysics. Subsequent sen-270 sitivity tests of liquid microphysical processes indicate that cloud liquid re-evaporation 271 plays a more important role in driving the convective invigoration than rain re-evaporation. 272 A process-level analysis reveals that higher cloud droplet number concentration slows 273 down the conversion of cloud liquid to rain, giving rise to an increase in cloud liquid re-274 evaporation and a decrease in rain re-evaporation, with the former outweighing the lat-275 ter. The net increase in the total re-evaporation is balanced by stronger condensation. 276 The dipole pattern of re-evaporative cooling above condensational heating is consistent 277 with the enhancement of convective mass flux. 278

279 Acknowledgments

Data and scripts used in this paper will be archived at ftp://data1.gfdl.noaa .gov/users/Xin.Rong.Chua/WRF_heat/WRF. We thank Tristan Abbott, Tim Cronin, Nadir Jeevanjee, Hugh Morrison, Ming Zhao, Hailey Shin, Usama Anber and Spencer Clark for helpful discussions, Shuguang Wang for providing the source code for the WRF model used in this study, and the developers of the "aospy" package. XRC was funded by the Cooperative Institute for Modeling the Earth System (CIMES) at Princeton University and the Singapore National Research Foundation.

287 **References**

- Abbott, T. H., & Cronin, T. W. (2020). A humidity-entrainment mechanism for microphysical invigoration of convection. *arXiv*.
- Albrecht, B. A. (1989, Sep 15). Aerosols, cloud microphysics, and fractional cloudi ness. Science, 245(4923), 1227.
- Andreae, M. O., Rosenfeld, D., Artaxo, P., Costa, A. A., Frank, G. P., Longo,
- K. M., & Silva-Dias, M. A. F. (2004). Smoking rain clouds over the Ama zon. Science, 303(5662), 1337–1342.

295	Chua, X. R., Ming, Y., & Jeevanjee, N. (2019). Investigating the fast response of
296	precipitation intensity and boundary layer temperature to atmospheric heating
297	using a cloud-resolving model. $Geophysical Research Letters, 46(15), 9183-$
298	9192. Retrieved from https://agupubs.onlinelibrary.wiley.com/doi/abs/
299	10.1029/2019GL082408 doi: 10.1029/2019GL082408
300	Emanuel, K. (2019). Inferences from simple models of slow, convectively coupled
301	processes. Journal of the Atmospheric Sciences (2019). doi: 10.1175/JAS-D-18
302	-0090.1
303	Fan, J., Rosenfeld, D., Yang, Y., Zhao, C., Leung, L. R., & Li, Z. (2015). Sub-
304	stantial contribution of anthropogenic air pollution to catastrophic floods in
305	Southwest China. Geophysical Research Letters, 42(14), 6066–6075.
306	Fan, J., Rosenfeld, D., Zhang, Y., Giangrande, S. E., Li, Z., Machado, L. A.,
307	others (2018). Substantial convection and precipitation enhancements by
308	ultrafine aerosol particles. Science, 359(6374), 411–418.
309	Fan, J., Yuan, T., Comstock, J. M., Ghan, S., Khain, A., Leung, L. R., Ovchin-
310	nikov, M. (2009). Dominant role by vertical wind shear in regulating aerosol
311	effects on deep convective clouds. Journal of Geophysical Research: Atmo-
312	<i>spheres</i> , <i>114</i> (D22).
313	Heikenfeld, M., White, B., Labbouz, L., & Stier, P. (2019). Aerosol effects on deep
314	convection: the propagation of aerosol perturbations through convective cloud
315	microphysics. Atmospheric Chemistry and Physics, 19(4), 2601–2627.
316	Hong, SY., Noh, Y., & Dudhia, J. (2006). A new vertical diffusion package with an
317	explicit treatment of entrainment processes. Monthly Weather Review, $134(9)$,
318	2318–2341.
319	Khairoutdinov, M., & Kogan, Y. (2000). A new cloud physics parameterization in
320	a large-eddy simulation model of marine stratocumulus. Monthly Weather Re-
321	$view, \ 128(1), \ 229-243.$
322	Langhans, W., Yeo, K., & Romps, D. M. (2015). Lagrangian investigation of the
323	precipitation efficiency of convective clouds. Journal of the Atmospheric Sci-
324	ences, 72(3), 1045-1062.
325	Lutsko, N. J., & Cronin, T. W. (2018). Increase in precipitation efficiency with sur-
326	face warming in radiative-convective equilibrium. Journal of Advances in Mod -
327	eling Earth Systems.

328	Morrison, H. (2012). On the robustness of aerosol effects on an idealized supercell
329	storm simulated with a cloud system-resolving model. $Atmospheric \ Chemistry$
330	and Physics, 12(16), 7689–7705.
331	Morrison, H., Thompson, G., & Tatarskii, V. (2009). Impact of cloud microphysics
332	on the development of trailing stratiform precipitation in a simulated squall
333	line: Comparison of one-and two-moment schemes. Monthly Weather Review,
334	137(3), 991-1007.
335	Noone, D. (2012). Pairing measurements of the water vapor isotope ratio with
336	humidity to deduce atmospheric moistening and dehydration in the tropical
337	midtroposphere. Journal of Climate, 25(13), 4476–4494.
338	Romps, D. M. (2014). An analytical model for tropical relative humidity. Journal of
339	Climate, 27(19), 7432-7449.
340	Rosenfeld, D., Lohmann, U., Raga, G. B., O'Dowd, C. D., Kulmala, M., Fuzzi, S.,
341	\ldots Andreae, M. O. (2008). Flood or drought: how do aerosols affect precipita-
342	tion? Science, $321(5894)$, $1309-1313$.
343	Stevens, B., & Feingold, G. (2009). Untangling aerosol effects on clouds and precipi-
344	tation in a buffered system. <i>Nature</i> , 461(7264), 607.
345	Storer, R. L., & van den Heever, S. C. (2013). Microphysical processes evident in
346	aerosol forcing of tropical deep convective clouds. Journal of the Atmospheric
347	Sciences, 70(2), 430-446.
348	Tao, WK., Chen, JP., Li, Z., Wang, C., & Zhang, C. (2012). Impact of aerosols
349	on convective clouds and precipitation. Reviews of Geophysics, $50(2)$.
350	Tao, WK., Li, X., Khain, A., Matsui, T., Lang, S., & Simpson, J. (2007). Role
351	of atmospheric aerosol concentration on deep convective precipitation: Cloud-
352	resolving model simulations. Journal of Geophysical Research: Atmospheres,
353	<i>112</i> (D24).
354	Twomey, S. (1974). Pollution and the planetary albedo. Atmospheric Environment,
355	8(12), 1251-1256.
356	van den Heever, S. C., Stephens, G. L., & Wood, N. B. (2011). Aerosol indirect
357	effects on tropical convection characteristics under conditions of radiative–
358	convective equilibrium. Journal of the Atmospheric Sciences, $68(4)$, $699-718$.
359	Wang, S., & Sobel, A. H. (2011). Response of convection to relative sea surface tem-

Geophysical Research: Atmospheres, 116(D11). 361

362	Williams, E., Rosenfeld, D., Madden	, N., Gerlach, J., Gears, N., Atkinson, L.,
363	others (2002). Contrastin	ng convective regimes over the Amazon: Implica-
364	tions for cloud electrification.	Journal of Geophysical Research: Atmospheres,
365	107(D20), LBA–50.	

366	Zhao, M., Golaz, JC., Held, I. M., Ramaswamy, V., Lin, SJ., Ming, Y., others
367	(2016). Uncertainty in model climate sensitivity traced to representations of
368	cumulus precipitation microphysics. Journal of Climate, $29(2)$, 543–560.

Table 1. Domain-average column-integrated condensation (*C*), total re-evaporation (*E*), rain re-evaporation (*ER*), cloud condensate re-evaporation (*EC*), accretion (*AR*), precipitation (*P*) in different cases. Also included is the re-evaporation efficiency (α). The differences between the control and perturbation simulations (the latter minus the former) are in parentheses. Except for α (unitless), all values are in mm day⁻¹. The last column ($\delta \alpha$) is based on a simple theory for $\delta \alpha$, i.e. $(1 - \alpha)\delta C/C$.

	C	E	ER	EC	AR	Р	α	$\widetilde{\delta \alpha}$
FU	13.7 (0.9)	9.1 (0.8)	3.7 (-0.7)	5.4(1.5)	8.2 (-0.6)	4.5(0.1)	$0.664 \ (0.014)$	0.022
LI	10.2(1.1)	5.8(1.0)	2.7 (-0.6)	3.1(1.6)	7.1 (-0.5)	4.5(0.1)	0.569(0.033)	0.046
RE	7.6(1.3)	2.8(1.3)	0.5 (-0.2)	2.3(1.4)	5.2 (-0.1)	4.7(0.1)	$0.368\ (0.092)$	0.108
CE	9.1 (0.5)	4.7(0.5)	2.7 (-0.6)	2.0(1.1)	7.1 (-0.6)	4.4(0.0)	$0.505\ (0.026)$	0.027

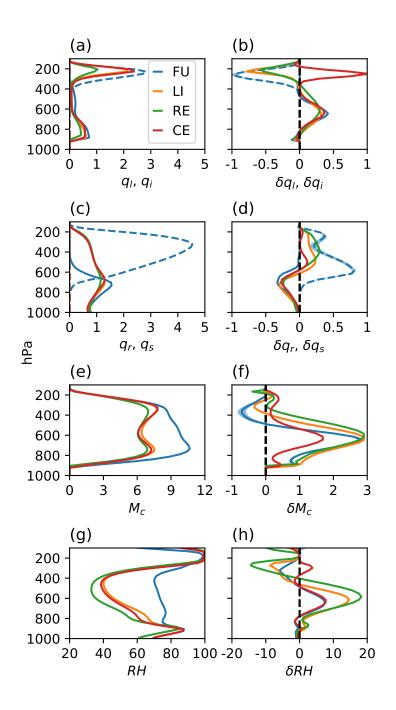


Figure 1. Vertical profiles of the domain-average (a)-(b) cloud liquid (solid, q_l , 10^{-5} kg⁻¹ kg⁻¹) or ice (dashed, q_i , 10^{-5} kg⁻¹ kg⁻¹) mixing ratio, (c)-(d) rain (solid, q_r , 10^{-5} kg⁻¹ kg⁻¹) or snow (dashed, q_s , 10^{-5} kg⁻¹ kg⁻¹) mixing ratio, (e)-(f) convective mass flux (M_c , g m⁻² s⁻¹) and (g)-(h) relative humidity (RH, %). The control experiments are in the left column, and the difference between the control and perturbation experiments are in the right column. The shading denotes the noise levels in FU. Note that cloud ice and snow are present only in FU and FU*

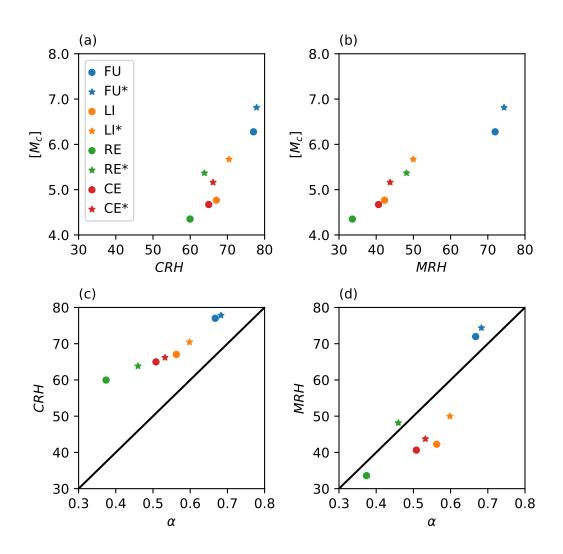


Figure 2. Scatter plots of (a) vertically averaged convective mass flux ($[M_c]$, g m⁻² s⁻¹) versus column relative humidity (CRH,%), (b) $[M_c]$ versus mid-tropospheric (400 to 600 hPa) relative humidity (MRH, %), (c) CRH versus the re-evaporation ratio (α , unitless), and (d) MRH versus α in all experiments.

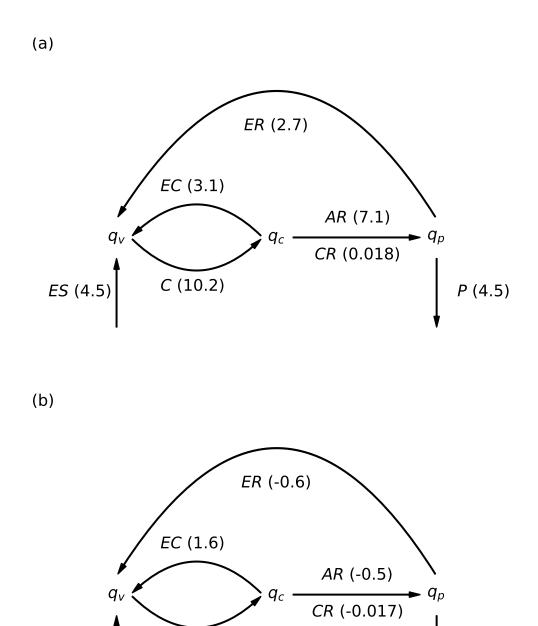


Figure 3. Domain-average column-integrated rates (mm day⁻¹) of microphysical processes involving water vapor (q_v) , cloud condensates (q_c) and hydrometeors (q_p) [condensation of cloud condensates (C), re-evaporation of cloud condensates (EC), conversion of cloud water to rain by autoconversion (CR) and accretion (AR) and re-evaporation of rain (ER)], as well as surface evaporation (ES) and precipitation (P). (a) is the LI control experiment, and (b) the difference between LI and LI^{*}. The corresponding values for all configurations are listed in Table 1.

P(0.1)

C (1.1)

ES (0.1)

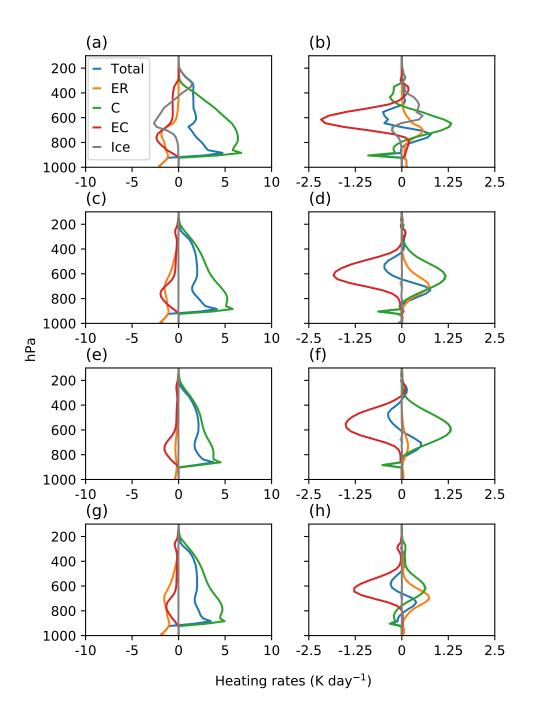


Figure 4. Vertical profiles of the domain-average heating rates (K day⁻¹) due to condensation (C), rain re-evaporation (ER), cloud condensate re-evaporation (EC), ice microphysics (Ice) and the total (Total). The control experiments are in the left column, and the difference between the control and perturbation experiments are in the right column. (a)-(b) are for FU, (c)-(d) for LI, (e)-(f) for RE, and (g)-(h) for CE.

Figure1.

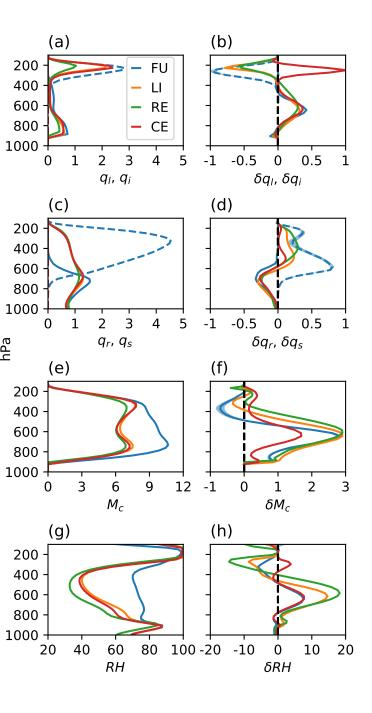


Figure2.

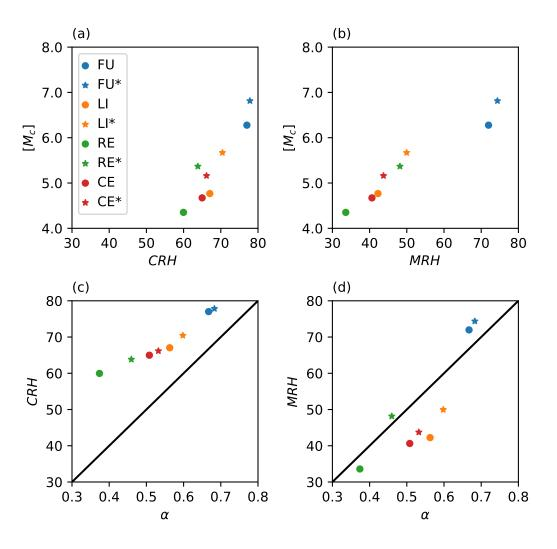
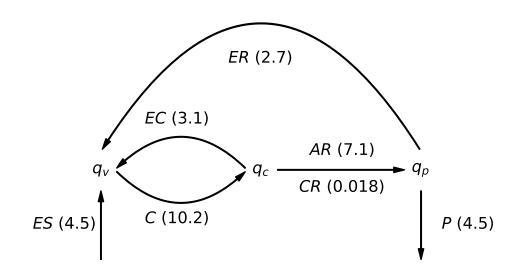


Figure3.





(b)

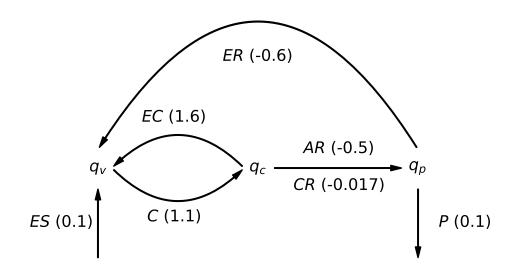
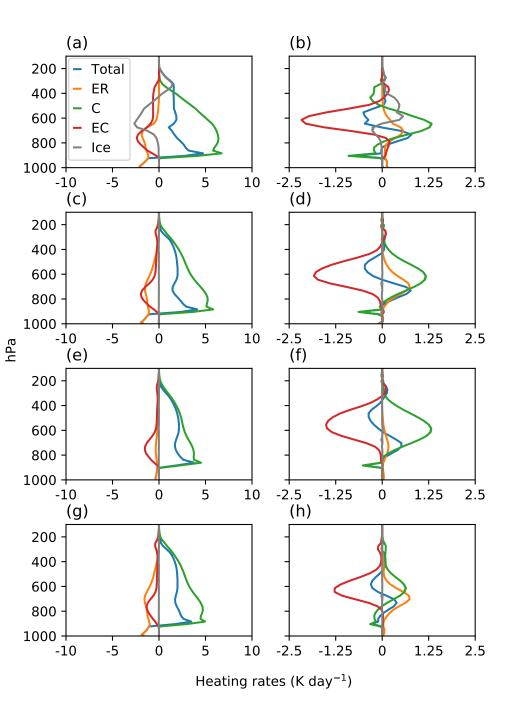


Figure5.



Supporting Information for "Convective invigoration traced to warm-rain microphysics"

Xin Rong Chua¹^{*}, Yi Ming^{1,2}

¹Program in Atmospheric and Oceanic Sciences, Princeton University, Princeton, New Jersey, USA

 $^2 {\rm Geophysical}$ Fluid Dynamics Laboratory, Princeton, New Jersey, USA

Contents of this file

1. Table S1

 * Current affiliation: Centre for Climate

Research Singapore, Singapore

January 15, 2020, 2:19am

Table S1. Additional ice processes included in the calculation of the terms in Table 1 in the

:

FULL cases.

Included in	Process
\overline{AR}	Cloud droplet accretion by snow
	Cloud droplet collection by graupel
	Cloud droplet collection by snow to graupel
	Accretion of cloud ice by snow
	Autoconversion of cloud ice by snow
	Ice-rain collection
	Ice-rain collision (added to snow)
	Conversion of large ice to snow
	Ice multiplication (rain and snow)
	Ice multiplication (rain and graupel)
EC	Sublimation of cloud ice
C	Deposition of cloud ice
	Primary ice nucleation
ER	Sublimation of graupel
	Sublimation of snow
	Evaporation of graupel
	Evaporation of snow
	Deposition of graupel
	Deposition of snow

January 15, 2020, 2:19am